Solid State Phenomena Vols 168-169 (2011) pp 177-184 *Online: 2010-12-30*

doi:10.4028/www.scientific.net/SSP.168-169.177

Magnetoelastic Effects in Nanostructures

J.I. Arnaudas[1, a], A. Badia-Majós[1, b], L. Berbil-Bautista[2, c], M. Bode[3, d], F.J. Castaño[4, e], M. Ciria[1, f], C. de la Fuente[1, g], J.L. Diez-Ferrer[1, h], S. Krause[5, i], B.G. Ng[4, j], R.C. O'Handley[4, k], C.A. Ross[4, l] and R. Wiesendanger[5, m]

[1]Dept. Física Materia Condensada - INA - ICMA, Univ. Zaragoza - CSIC, 50071 Zaragoza, Spain

[2]Materials Sciences Division, Lawrence Berkeley National Lab., Berkeley, CA 94720-7300, USA

[3]Center for Nanoscale Materials, Argonne National Laboratory, Argonne, Illinois 60439, USA

[4]Dept. of Materials Science and Engineering, Massachusetts Institute of Technology, Cambridge, MA 02139, USA

[5]Institute of Applied Physics, University of Hamburg, Jungiusstr. 11, D-20355 Hamburg, Germany

[a]arnaudas@unizar.es, [b]anabadia@unizar.es, [c]lberbil@googlemail.com, [d]mbode@anl.gov, [e]fer@mit.edu, [f]ciria@unizar.es, [g]cesar@unizar.es, [h]jlx@unizar.es, [i]skrause@physnet.uni-hamburg.de, [j]bryan.ng@gmail.com, [k]bobohand@mit.edu, [l]caross@mit.edu, [m]rwiesend@physnet.uni-hamburg.de

Keywords: Magnetoelasticity, anisotropy, nanostructures, Dy films, Ni nanowires,

Abstract. Understanding of the relationship between stress and magnetic properties in nanostructures is of both fundamental and practical interest. In the present paper, we illustrate this statement with some recent research results. First, we will see how the magnetoelastic interaction in Dy films controls the magnetic structure at the nanoscale due to the presence of the structural defects and their associated strain fields. Then, it will be shown how the magnetoelastic contribution can dominate the total anisotropy in epitaxial (100) oriented Cu/Ni/Cu nanowires, where the film patterning process performed to produce the nanowires induces strain changes large enough to favor a net in-plane anisotropy transverse to the lines.

Introduction

It has been shown that the strain associated with linear defects efficiently controls the domain wall pinning by means of the magnetoelastic (ME) interaction, with only a few of such defects needed to stabilize the large-area domain structure in ultrathin films [1]. Rare-earth metals are of great interest for studies of the ME interaction, since it is particularly strong in this class of materials. Previous studies [2] showed that the "large-scale" magnetic structure of Dy films is dominated by the density of linear defects that evolve during the film growth. Particularly, strong ME effects are seen several tens of nanometers around the core of a dislocation, i.e. at distances smaller than the corresponding decay length of the strain fields in metals. In a recent work [3] we showed that, at this length scale, the magnetic structure is governed by the competition between the exchange coupling and ME interaction.

The control of the magnetic anisotropy (MA) and domain configurations in lithographically defined magnetic elements with submicron lateral dimensions is of importance for spintronic devices. Planar nanowires (NWs), in particular, have been investigated in view of their potential use in domain wall (DW) devices proposed for data storage and logic applications. The magnitude and direction of the net MA determine the domain structure and DW type of a patterned element. MA is commonly controlled via the geometry of the structure, or by magnetocrystalline (MC) anisotropy, but in certain strained epitaxial magnetic films, the ME effects can dominate over the anisotropy. In the epitaxial (100) oriented Cu/Ni 9-10-15 nm/Cu planar NW's we have quantified the patterning-induced changes in the MA and hysteresis. The strain relaxation leads to a thickness-dependent net in-plane anisotropy transverse to the lines, which we explain by considering the patterning-induced

changes in the ME anisotropy, combined with the shape and MC anisotropies [4]. Thus, by tailoring the film thickness and wire orientation, the easy axis direction of the NW's may be controlled.

Magnetic Structure at the Nanoscale in Dysprosium Films

Experimental details. Continuous and flat (0001) terminated Dy films were grown on W(110) following the process described in [2]. The SP-STM experiments were performed in an ultrahigh-vacuum system at temperatures between 20 and 60 K. To obtain magnetic contrast, the tips were coated by at least 100 atomic layers (ALs) of antiferromagnetic Cr, or dipped into the Dy film to obtain a Dy cluster on the tip apex, as described in [5]. These two methods result in tips preferentially magnetized parallel to the sample's surface plane. The magnetic signal was measured by mapping the spin-resolved differential tunneling conductance dI/dU as a function of lateral position of the tip. This dI/dU signal was recorded by lock-in detection of the current modulation that results from adding a modulation voltage U_{mod} = 25 mV_{rms} to the sample bias and is proportional to the projection of the local magnetization of the sample, $\boldsymbol{m}_s$, onto the tip magnetization, $\boldsymbol{m}_t$, at any given position of the surface [6-7].

SP-STM results. Fig. 1(a) shows an STM topograph of a 90 AL film of Dy. The surface presents monoatomic steps that separate atomically flat terraces. Two steps always merge at the position where a screw dislocation with a Burgers vector [0001] pierces the surface (white arrows in Fig. 1.) [2]. Within the atomically flat terraces highly asymmetric depressions are found that—by means of atomically resolved STM—were identified as the points where edge dislocations with the Burgers vector $[2\bar{1}\bar{1}0]$ emerge on the surface [2] (white circles in Fig. 1(a-b)). The comparison of the positions of the line defects observed in the STM topograph in Fig. 1(a) with the magnetic signal map in Fig. 1(b) reveals that both kinds of defects result in strong pinning of the domain walls [2]. In most cases, several domains meet at the position of the pinning center, as, e.g., in the lower right corner of Fig. 1(b), where three domains meet at the position of an edge dislocation.

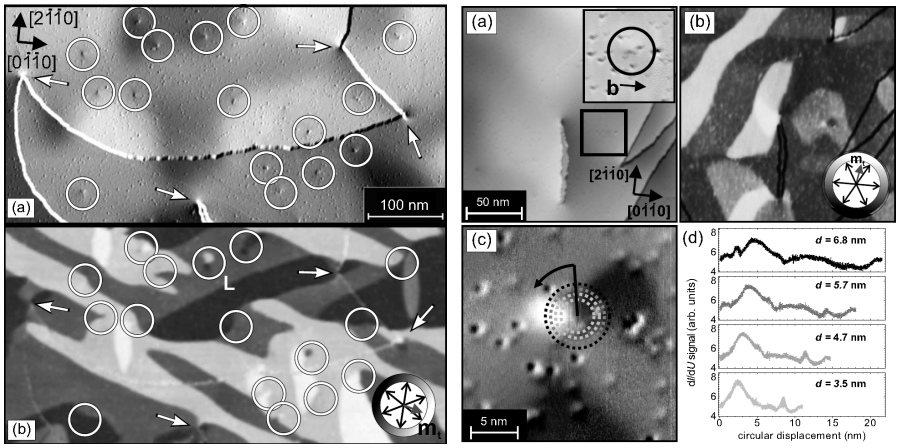

Fig. 1. (left) (a) STM topograph and (b) magnetic signal map of a 90 AL Dy film. The schematic inset summarizes the different magnetic contrast levels which result from different projections of $\boldsymbol{m}_s$ onto $\boldsymbol{m}_t$ calculated as in [2], The arrows (circles) mark the position where screw (edge) dislocation appear on the surface.

Fig. 2. (right) (a) STM topograph and (b) magnetic signal map of a region where an edge dislocation is localized within a single domain. (c) Detail of the neighborhood of the dislocation. (d) Circular line sections marked in (c).

These patterns often resemble the spin structure formerly observed around magnetic vortex cores [5] with a continuous in-plane magnetization in close proximity to the dislocation site. Occasionally, other features consisting of a lobe-like structure surrounded by a single ferromagnetic domain are found, as the one marked with an "L" in Fig. 1(b). This feature is discussed in greater detail in Fig. 2, where an edge dislocation is located within a single domain. Panel 2(a) shows the topography of the area (the direction of the Burgers vector is indicated in the inset). Fig. 2(b) shows a magnetic signal map taken simultaneously with Fig. 2(a). The schematic inset summarizes the different magnetic contrast levels which result from different projections of $\boldsymbol{m}_s$ onto $\boldsymbol{m}_t$ (the latter forming an angle of 82º with the Burgers vector). Based on the analysis presented in [2], we obtain an angle of 98±5º between the magnetization direction of the large domain in the square and $\boldsymbol{m}_t$. The closer view in Fig. 2(c) shows that a single insulated dark-bright lobe structure emerges from the disloca-

tion core. It extends about 10 nm into the surrounding domain. The circular line sections of the magnetic signal taken at different distances from the dislocation core shown in Fig. 2(d) reveal a continuous behavior of the magnetic signal with extremes of the canting angles in the lobes of 45±15° and 170±15° in the brightest and the darkest regions.

Calculation of the observed magnetic nanostructures. In order to interpret the observed magnetic structures and to analyze the driving forces generated by the linear defect, we have calculated the spin directions of an ensemble of atoms surrounding an edge dislocation. In physical terms, the interaction between the stress field occurring around a dislocation line and the spontaneous magnetostrictive strains existing in a ferromagnet gives rise to a ME energy which, together with exchange, dipolar, anisotropy, and elastic energies, determine the magnetic configuration in the neighborhood of the linear defect. In uniformly strained materials, the distortion of the lattice tends to align the magnetic moments along certain directions. However, as we shall see below, the nonuniform stress field of the dislocation results in a canting of the magnetic moments near the dislocation cores, which act as nucleation centers for the observed magnetic domains and other magnetic nanostructures, like the above mentioned lobes.

In our calculation we consider a ferromagnetic domain in a Dy film, having its magnetization parallel to one of the easy magnetization axes (*a* directions) in the basal plane (BP) of the Dy hexagonal close-packed (hcp) crystal structure. We assume a single edge dislocation with the Burgers vector $\vec{b} = [2\bar{1}\bar{1}0]a$ and a dislocation line running perpendicular to the BP through the whole film thickness. The numerical study of the spin configuration was performed by using an hcp arrangement of magnetic ions and considering translational symmetry along the direction perpendicular to the film plane, i.e., to the BP of the hcp structure. A hexagonal two-dimensional (2D) lattice consisting of a set of ion sites was used. In the center of the mesh we define the origin of a Cartesian coordinate system (OXY), where the core of a pure edge dislocation running along the *z* axis is located. This extra plane located at $y > 0$ produces a stress field which essentially compresses the upper half of the mesh and tenses the lower one. The stress field produced by this linear defect depends on the crystal structure. For an hexagonal crystal the non-null components of the stress tensor, $\overleftrightarrow{\sigma}(\mathbf{r})$, are (see, e.g. ref. [8]), $\sigma_{xx} = -y(ax^2 + by^2)/u(x,y)$, $\sigma_{yy} = y(gx^2 - hy^2)/u(x,y)$, $\sigma_{xy} = \sigma_{yx} = x(ex^2 - fy^2)/u(x,y)$ and $\sigma_{zz} = y(px^2 + qy^2)/u(x,y)$, where $u(x,y) = x^4 + sx^2y^2 + ty^4$ and the coefficients of the x and y coordinates are combinations of the hexagonal elastic constants of the material and include the Burger's vector modulus, $|\vec{b}| = b_x = 3.2$ Å, in our case. This strongly anisotropic stress field which decays with distance ($\sigma_{ij} \propto 1/r$) couples with the magnetization via the ME interaction and can be described by a local anisotropy field which is to be added to the MC anisotropy. Thus, the free energy of a layer of Dy ions can be written as the sum of: (i) the basal-plane anisotropy energy, F_{CEF}, which originates from the crystal electric field (CEF), (ii) the ME energy, F_{ME}, associated with the non-null strains, (iii) the dipolar energy, F_D, and (iv) the exchange energy, F_{EX}. As the first approximation, $F_{CEF} \simeq \sum_i K_6^6 \cos(6\varphi_i)$, where K_6^6 is the hexagonal BP pure CEF anisotropy constant and φ_i is the angle formed by the *i*th spin direction and the hcp easy axis, ***a***. The ME energy per ion, located at $\mathbf{r}_i$, may be written in the form $-\overleftrightarrow{\epsilon}(\mathbf{r}_i) : \overleftrightarrow{\sigma}(\mathbf{r}_i) \equiv -\sum_{kl} \epsilon_{kl}(\mathbf{r}_i)\sigma_{kl}(\mathbf{r}_i)$, where $\overleftrightarrow{\epsilon}(\mathbf{r}_i)$ is the local magnetostrictive strain tensor which depends on the strength of the ME interaction and on the spin direction at $\mathbf{r}_i$ [9] and $\overleftrightarrow{\sigma}(\mathbf{r}_i)$ is the internal stress tensor caused by the dislocation. In our case $F_{ME} = -\sum_i [\lambda_{100}(\sigma_{xx}^i \cos^2\varphi_i + \sigma_{xy}^i \sin 2\varphi_i + \sigma_{yy}^i \sin^2\varphi_i) + \lambda_{101}\sigma_{zz}^i]$, where λ_{100} and λ_{101} are the magnetostriction constants. The classical dipolar interaction gives rise to the energy $F_D = (\mu_0/4\pi) g^2 \mu_B^2 \sum_{i>j} \{[\boldsymbol{J}_i \cdot \boldsymbol{J}_j] r_{ij}^{-3} - 3[(\boldsymbol{J}_i \cdot \mathbf{r}_{ij})(\boldsymbol{J}_j \cdot \mathbf{r}_{ij})] r_{ij}^{-5}\}$,

where $\boldsymbol{r}_{ij}$ is the vector between spin sites i and j, μ_0 is the permeability of the vacuum, g is the Landé factor (4/3 for Dy), J is the total angular momentum (15/2 for Dy), and μ_B is the Bohr magneton. Finally, $F_{\mathrm{EX}} = -(\Im/2)\sum^{*}_{i,j} \boldsymbol{J}_i \cdot \boldsymbol{J}_j$, $\Im$ being the ferromagnetic exchange constant and the symbol " * " indicating that each ion is exchange coupled only to its six nearest neighbors. Minimization of the total energy $F_{\mathrm{CEF}} + F_{\mathrm{ME}} + F_{\mathrm{D}} + F_{\mathrm{EX}}$ allows us to obtain the equilibrium configurations of magnetic moments around the edge dislocation. As constraints we used the periodic boundary conditions with a fixed moment direction at the sample boundaries and constant modulus for all atomic sites. This means that we are analyzing the effect of an edge dislocation located in the center of a single magnetic domain with equal spins which would be otherwise ferromagnetically aligned along one of the easy directions, $\boldsymbol{a}$. The variational problem has been solved numerically by means of the FORTRAN package LANCELOT that implements a globally convergent augmented Lagrangian algorithm [10] that allows avoiding spurious local minima. Since the studied Dy film, at T = 58 K, clearly displays ferromagnetic order within the BP, the calculations have been performed by using the values of $\Im$, K_6^6, and λ_{100} of bulk Dy, i.e., $\Im = 1.8\times10^7$ erg/cm^3, [11] $K_6^6 = -3.0\times10^6$ erg/cm^3, [12] and $\lambda_{100} = 8.1\times10^{-3}$ [13] The elastic constants appearing in the coefficients of the components of the stress tensor, $\overleftrightarrow{\sigma}(\boldsymbol{r}_i)$, are taken from [14]. The minimization of the free energy F leads to magnetic domains which extend indefinitely from the dislocation core (see Fig. 3(a), where the projection of the Dy spins onto $\boldsymbol{m}_t$ corresponding to the experimental conditions in Fig. 2 is plotted). This result, which does not depend on the size of the 2D lattice up to 250×250 ion sites, is consistent with most of the cases found around edge dislocations (see Fig. 1(b)), and points out to the dislocations as nucleation and pinning sites for the magnetic domains. However, it does not explain the relatively small size of the structure shown in Fig. 2. Only after adding a Zeeman energy equivalent to the effect of an in-plane magnetic field of about 1 kOe to the free energy F, we were able to reproduce the experimental finding of Fig. 2.

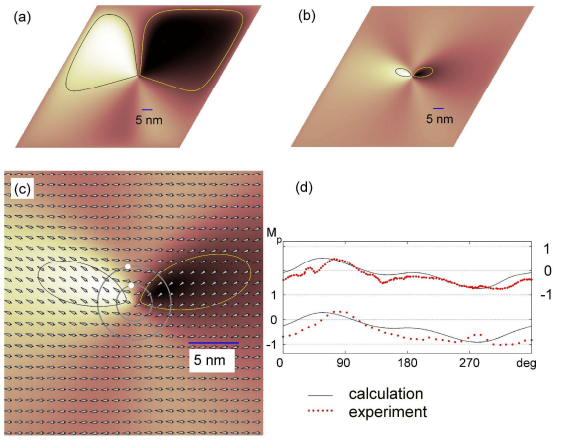

Fig. 3. (Color online) (a) Calculated dI/dU map, using a 250×250 lattice, corresponding to the experimental conditions in Fig. 2. Two level contours are marked upon the lobes for visual purpose. (b) The same as for (a), with stabilizing field (see text for details). (c) Vector plot of the theoretical magnetic moments in the vicinity of the edge dislocation [75×75 sites, central part of (b)]; for clarity, a simplified mesh is represented. Panels (d) correspond to the circular CCW line sections, in the horizontal axis the angle in degrees starting from the white dots and in the vertical axis the magnetic signal in arbitrary units, shown in (c), at d = 7 nm and d = 3.5 nm.

A possible origin of this in plane magnetic field may be the magnetic sandwich structure of Dy films on W (110). Indeed, it has been observed by means of resonant soft X-ray scattering in a 180 AL Dy film on W (110) that the low temperature (T < 125 K) magnetic profile of the film is rather complex [15]. Figure 3(b) shows the results of the new calculation and Fig. 3(c) shows the direction of the spins in a 75x75 ion sites region. The calculation recovers the extension of the observed magnetic structure and its general shape. Furthermore, Fig. 3(d) shows direct comparison of the magnetic signal from the experimental data and the calculated one, for two circular-line sections at d = 7 nm and d = 3.5 nm. The agreement is quite good, particularly if we consider that in the parts where deviations occur we observe (see Fig. 3) the presence of adsorbates in the sample that clearly distort the magnetic image. The extrema of the magnetization canting angles in the calculation are 58° and

138° and are in reasonable agreement with the previously mentioned experimental values (notice that these extrema are located at around 61° and 280° in the circular line sections of Fig. 3).

Cu/Ni/Cu planar nanowires. The in-plane anisotropy energy of a NW made from a single-crystal cubic material includes the MC anisotropy $K_1\cos^2\phi\sin^2\phi$ plus the ME and magnetostatic contributions $(K_{me}+K_{sh})\sin^2\phi$, a uniaxial term, where ϕ is the angle between the magnetization M and the NW axis. The shape energy term can be written as $K_{sh} = 0.5\,\mu_0\,(N_y - N_x)M^2$ (we assign x||NW axis and y ⊥NW axis; thus N_y and N_x are, respectively, the transverse and longitudinal demagnetization factors). Because K_{sh} is always positive (giving an easy direction along the NW axis), the in-plane uniaxial anisotropy term will depend on the sign of the ME coefficient K_{me}. If $K_{me} > 0$ the uniaxial anisotropy along the NW is enhanced, as observed in magnetic semiconductors such as (Ga,Mn)As/(In,Ga)As [16], while if $K_{sh} < -K_{me}$, the uniaxial anisotropy drives M transverse to the NW axis. For cubic thin-film materials grown on the (001) plane, $K_{me} = -B_1\varepsilon_\gamma$, where B_1 is the ME stress coefficient and $\varepsilon_\gamma = \varepsilon_{xx} - \varepsilon_{yy}$ is the strain associated with the breaking of the in-plane fourfold symmetry. The sign of ε_γ in a patterned heteroepitaxial system can be obtained by considering two factors: first, the strain relaxation in a NW is larger along the direction transverse to the NW axis so $|\varepsilon_{xx}| > |\varepsilon_{yy}|$ and, second, the misfit between the substrate lattice parameter a_s and the lattice parameter of the magnetic material a_m determines the sign of ε_{xx} and ε_{yy}, so that $a_m >(<) a_s\varepsilon_{xx}$, $\varepsilon_{yy} <(>) 0$ and $\varepsilon_\gamma <(>) 0$. The Ni/Cu(001) system, which has $B_1 > 0$ and $a_{Ni} < a_{Cu}$, can meet the criterion $-K_{me} = B_1\varepsilon_\gamma > K_{sh}$ and is therefore able to produce NWs with magnetization in-plane but transverse to the wire axis. We have shown previously that patterning Cu/Ni/Cu(001) epitaxial films of 6.9 and 20.6 nm Ni thickness can indeed lead to NWs with a net transverse anisotropy [17].

Experimental details. Epitaxial Cu(5 nm)/Ni(t_{Ni})/Cu(100 nm) films with t_{Ni} between 2 and 15 nm were grown on Si (001) wafers at room temperature by electron-beam evaporation in a chamber with a base pressure below $2\text{x}10^{-10}$ Torr, using a procedure reported elsewhere [18]. The single-crystal nature of each layer and the epitaxial relationships, i.e., Si ⟨100⟩ //Cu ⟨110⟩ //Ni ⟨110⟩, are observed in situ by reflection high-energy electron diffraction (RHEED) [4] and high resolution grazing incidence X-ray diffraction, done in the BM25B beamline of ESRF using a photon energy of hν =15 keV. The magnetic properties of the samples were investigated by alternating gradient magnetometry, vibrating sample magnetometry, and magnetic force microscopy, using a low-moment tip. In addition to the anisotropy calculation based on strain, an estimate of the effective magnetic anisotropy constants was also made from the difference between magnetization loops measured along specific directions [19]. To eliminate the effect of hysteresis, the anhysteretic *M-H* curve is calculated by averaging the descending and ascending branches of the hysteresis loop at constant values of M. Arrays of Cu/Ni/Cu NW's with the wire axis along the Ni ⟨100⟩ direction were fabricated by ion-beam etching (see Fig. 4), using a Ta grating as a hard mask. The Ta was patterned using interference lithography [20] and reactive ion etching to form a polymer grating from a trilayer resist stack, then sputtering and liftoff of Ta to form the hard mask. We fabricated four NW arrays with t_{Ni} = 4, 9, 10, and 15 nm, which will be labeled as 4NW, 9NW, 10NW, and 15NW, respectively. Samples 9NW, 10NW, and 15NW have a period close to 450 nm and a wire width of 300, 200 and 200 nm, respectively, while 4NW had a period of 800 nm and a wire width of 600 nm.

Magnetism and strain in the nanowires: results and discussion. Magnetometry shows that the unpatterned nickel films exhibit out-of-plane magnetization, with an effective perpendicular magnetic anisotropy $K_p > 0$, for t_{Ni} between about 1.5 and 11.5 nm (see Fig. 1 in ref. [4]). The 4-, 9-, and 10-nm-thick films are more easily magnetized out-of-plane compared to in-plane ($K_p > 0$) while for the 15 nm film the opposite behavior is observed ($K_p < 0$). Figure 4 shows data for the patterned films. The in-plane loops with H applied along the x and y directions provide information about the effects of patterning on the magnetic behavior. These samples span the range from high K_p (t_{Ni} = 4 nm) to a regime (t_{Ni} = 9, 10, and 15 nm) where K_p is low and its sign changes from positive to negative. For 4NW, $K_p > 0$, while for 9NW, 10NW, and 15NW, $K_p < 0$, showing that K_p has

changed sign for $t_{Ni} = 9$ and 10 nm. For the three samples with negative K_p the hysteresis loops suggest that M is oriented preferentially in plane, transverse to the nanowires, particularly for the 10NW and 15NW samples. This result, which is consistent with our prior work [17], is contrary to what would be expected from shape anisotropy alone, and demonstrates the governing effect of K_{me}.

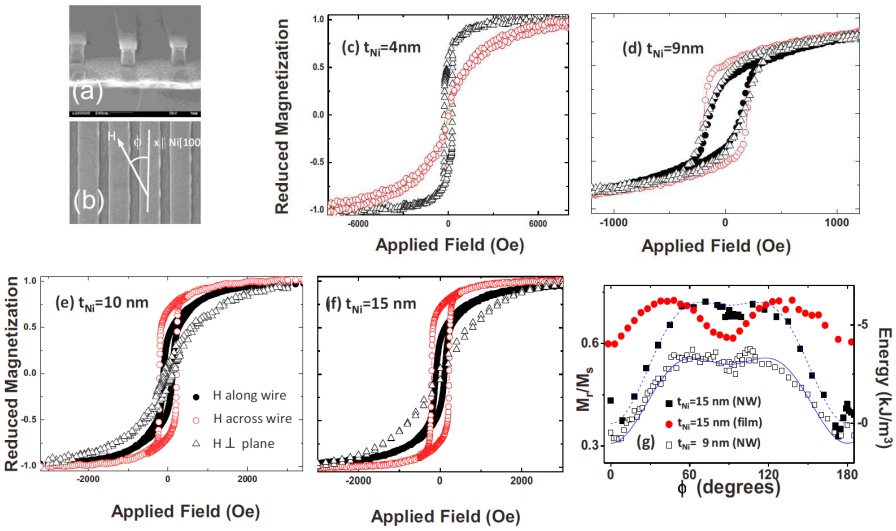

Fig. 4. (Color online) (a) SEM images of grating pattern of resist on the magnetic films and (b) NW sample after hard mask deposition and ion-beam etching. $M(h)$ loops for NW arrays with nickel thickness equal to 4 (c), 9 (d), 10 (e), 15 nm (f). Triangles indicate $H \perp$ to the film plane, open circles correspond to H transverse to the NW axis and full symbols indicate H||NW array. For the 4NW sample the two in-plane loops are equivalent and only one loop is represented; (g) angular variation in M_r/M_s for the 15NW (solid squares), and the 9NW (empty squares) arrays and the 15-nm-thick film (circles); the dashed line is $E_{anis}(\phi)$ with $K_u = -6$ kJ/m^3 and $K_1 = -10$ kJ/m^3 and the continuous line is $E_{anis}(\phi)$ with $K_u = -4$ kJ/m^3 and $K_1 = -7$ kJ/m^3 shifted by a constant value to fall on the 9NW data.

A direct measurement of the strain asymmetry is required to quantify the ME anisotropy. This was performed for sample 10NW. The strain state in the 10NW array was determined from the X-ray diffraction reciprocal space mapping in the vicinity of the asymmetric (402) and (042) Bragg reflection from Cu and Ni layers [4]. These scans are sensitive to the lattice parameter a_x parallel to the NW axis and a_y transverse to the NW axis, as well as to the out-of-plane lattice parameter. From the experimental positions of the maxima of the scattered intensity the in-plane lattice constants were determined as $a_x = 3.553$ Å, $a_y = 3.541$ Å, and $a_z = 3.504$ Å leading to $\varepsilon_{xx} = (8.3\pm0.1) \times 10^{-3}$, $\varepsilon_{yy} = (4.9\pm0.1) \times 10^{-3}$, and $\varepsilon_{zz} = (-5.7\pm0.1) \times 10^{-3}$, respectively. The ε_{xx} of the 10NW sample is close to the value found for the unpatterned films while ε_{yy} is about half as large [4], indicating that the nanowires undergo a relaxation transverse to the NW axis. Considering the z direction, ε_{zz} is smaller than the value $\varepsilon_{zz} \approx -12.8\times10^{-3}$ calculated for the biaxially stressed unpatterned film ($\varepsilon_{zz} = -2(c_{12}/c_{11})\,\varepsilon_{xx}$, where the c's are the nickel elastic constants and $\varepsilon_{xx} \approx -10\times10^{-3}$) [18], showing that ε_{zz} is also relaxed in the NW array. Based on $\varepsilon_\gamma = \varepsilon_{xx} - \varepsilon_{yy} \approx (3.4 \pm 0.2)\times10^{-3}$ for sample 10NW, we obtain $K_{me} = -21\pm2$ kJ/m^3 [with $B_1 = 6.2$ MPa (Ref. [21])]. K_{sh} was determined by using the demagnetizing factors for arrays of planar NWs reported in [22]. With $N_x = 0$ and $N_y = 0.91 t_{Ni}/w$ (w = width) for the array, a value slightly smaller than that of a single infinite NW, $K_{sh} = 6.6$ kJ/m^3 for sample 10NW. These values imply $K_u = -14.4$ kJ/m^3 which quantifies the transverse anisotropy in terms of a ME effect due to asymmetrical relaxation of the in-plane epitaxial lattice strain. An estimate of K_u may also be obtained from the anhysteretic M-H curves measured in the longitudinal and transverse directions [19]. This yields K_u (15NW) = −6.0 kJ/m^3; K_u (10NW) = −6.3 kJ/m^3, and K_u (9NW) = −4.0 kJ/m^3. The value for 10NW is in reasonable agreement with that calculated from the measurement of the strain, considering the approximations of the estimate based on hysteresis. The NWs were patterned such that the ⟨100⟩ in-plane directions are parallel to the NW axis, and the ⟨110⟩ in-plane directions, which are magnetically easy according to the MC anisotropy, form an angle of 45° to the NW axis. Thus, a competition between the uniaxial term and the MC contribution is expected. To elucidate that competition we examine the symmetry of the in-plane

magnetic anisotropy. Figure 4(g) presents the variation in the remanence ratio M_r/M_s as function of the angle φ between the NW axis (x axis) and H for the 9NW and 15NW arrays and for the 15 nm unpatterned film, in which $\varphi = 0$ corresponds to a $\langle 100 \rangle$ direction. As expected, for the unpatterned film, M_r/M_s displays a fourfold dependence on φ. The $\langle 110 \rangle$ directions, at 45° to the NW axis, are the in-plane easy axes. M_r/M_s takes maximum and minimum values along the $\langle 110 \rangle$ easy and $\langle 100 \rangle$ hard axes, respectively, defined by the MC anisotropy $K_1 \cos^2\phi \sin^2\phi$ with $K_1 = -4.5$ kJ/m^3 [21].

For the 9NW and 10NW arrays the in-plane $\langle 110 \rangle$ direction is no longer the easy in-plane direction. Instead, the maximum values of M_r/M_s are near $\varphi = 70°$, although the difference between the values for M_r/M_s at ϕ=70° and 90° is small. The minimum value for M_r/M_s is at $\varphi = 0°$. In the (001) plane, the total anisotropy energy can be modeled as the sum of a uniaxial term, comprising shape and ME contributions, and the MC contribution: $E_{anis}(\phi)=K_u \sin^2\phi+K_1 \cos^2\phi \sin^2\phi$. The minimum for E_{anis} depends on the K_u/K_1 ratio. If both constants are negative, for $|K_u| > |K_1|$ the minimum is at 90°, whereas if $|K_u| < |K_1|$ the minimum is given by $\cos 2\phi = -K_u/K_1$.

Taking the value at which M_r/M_s has its maximum value as the minimum of $E_{anis}(\phi)$ and using the value of K_u obtained from the hysteresis loops and strain data, we obtain, $K_1 \sim -7.5$ and -18.4 kJ/m^3, respectively, for sample 10NW. This suggests that K_1 is greater than the MC anisotropy of bulk Ni, which is -4.5 kJ/m^3. An enhancement of K_1 in nickel thin films has been reported [23-24] and its origin linked to a magnetoelastic contribution due to the isotropic in-plane stress in the film arising from the misfit between the substrate and film. The lines in Fig.4(g) represent $E_{anis}(\phi)$ calculated for the 9NW and 15NW arrays, and show excellent agreement with the measured angular dependence of the ratio M_r/M_s indicating the presence of a uniaxial term in E_{anis}.

Magnetic force microscopy was used to clarify the domain structure and aid in the interpretation of the anisotropy data. The results obtained with this technique [4] were consistent with a magnetization transverse to the wire length, as suggested by the hysteresis loops.

Finally, we reconsider the strain data to show why K_p decreases on patterning: K_p includes the ME term $-B_1[\varepsilon_{zz}-0.5(\varepsilon_{xx}+\varepsilon_{yy})]$ and the components of strain decrease on patterning. For an unpatterned Ni film in biaxial stress, the magnetoelastic contribution to anisotropy reduces to $B_1\varepsilon_{xx}[1+2(c_{12}/c_{11})]$, with $B_1 = 6.2$ MPa and the ratio $c_{12}/c_{11} = 0.64$. This gives a value for the ME contribution of 141 kJ/m^3 for the 10-nm-thick film in which $\varepsilon_{xx} = 0.01$. For the 10NW sample, we use for the strain components the values measured by X-ray diffraction. We find that the ME contribution to K_p is 76 kJ/m^3, showing that K_p must have decreased by about 65 kJ/m^3 upon patterning. This decrease is larger than the net K_p of the unpatterned film, which was about 10 kJ/m^3. This explains why K_p becomes negative in the 9 and 10-nm-thick patterned NWs despite being positive for the unpatterned films. In contrast, for the 4-nm-thick sample, the K_p of the unpatterned film was about 90 kJ/m^3, so, the strain relaxation is insufficient to drive the net anisotropy in plane, and the patterned 4NW sample retains its out-of-plane anisotropy.

Conclusions

We have shown, through two particular examples, how the magnetoelastic energy can dominate in the behavior of a magnetic system. Firstly, at the nanoscale level, the magnetic structure around single line defects in Dy/W (110) films, as seen via spin-polarized STM, is analyzed by means of micromagnetic calculations. The presence of complex spin structures is quantitatively explained by the strong changes in magnetic easy axis driven by the coupling of the magnetoelastic energy and the deformation field around the dislocation core. The second case deals with the macroscopic magnetic behavior of planar nanowire arrays made from heteroepitaxial Cu/Ni/Cu thin films, with a range of Ni film thicknesses. We have quantitatively analyzed their magnetoelastic, shape and magnetocrystalline anisotropies and showed that the patterning of the continuous films leads to anisotropic stress relief and a magnetoelastic anisotropy which dominates the net magnetic anisotropy of

the Ni nanostructures. These results show how magnetoelastic effects may be used to control the magnetic domain structure and the net anisotropy, helping in the design of nanostructured devices.

Financial support from the Spanish MCyT Project No. NAN2004-09183-C10-10, the MICINN Project No. MAT2006-07094, the DGA Grants No. E81 and No. PI049/08, the DFG (SFB 668 and grant BO1468/17–1), the ERC Advanced Grant "FURORE", the DOE Contract No. DEAC02-06CH11357, the Fondo Social Europeo and the Singapore-MIT Alliance is gratefully acknowledged. We thank B. Pita, V. García, and F. Ilievski for their help in this work. We acknowledge the European Synchrotron Radiation Facility for provision of synchrotron radiation facilities and we would like to thank the staff at Spline for assistance in using beamline BM25.

References

[1] L. Krusin-Elbaum, T. Shibauchi, B. Argyle, L. Gignac and D. Weller: Nature Vol. 410 (2001), p. 444-446.
[2] S. Krause, L. Berbil-Bautista, T. Hanke, F. Vonau, M. Bode and R. Wiesendanger: Europhys. Lett. Vol. 76 (2006), p. 637-643. L. Berbil-Bautista, S. Krause, M. Bode and R. Wiesendanger, Phys. Rev. B Vol. 76 (2007), p. 064411.
[3] L. Berbil-Bautista, S. Krause, M. Bode, A. Badia-Majos, C. de la Fuente, R. Wiesendanger and J. I. Arnaudas: Phys. Rev. B Vol. 80 (2009), p. 241408.
[4] M. Ciria, F. J. Castano, J. L. Diez-Ferrer, J. I. Arnaudas, B. G. Ng, R. C. O'Handley and C. A. Ross: Phys. Rev. B Vol. 80 (2009), p. 094417.
[5] R. Wiesendanger: Rev. Mod. Phys. Vol. 81 (2009), p. 1495-1550, and references therein.
[6] J. C. Slonczewski: Phys. Rev. B Vol. 39 (1989), p. 6995-7002.
[7] D. Wortmann, S. Heinze, P. Kurz, G. Bihlmayer and S. Blugel: Phys. Rev. Lett. Vol. 86 (2001), p. 4132-4135.
[8] J. P. Hirth and J. Lothe: *Theory of Dislocations*. (Krieger, Malabar, FL, 1992).
[9] E. Callen and H. B. Callen: Phys. Rev. Vol. 139 (1965), p. A455-&.
[10] A. R. Conn, N. I. M. Gould and P. L. Toint: *LANCELOT : a Fortran package for large-scale nonlinear optimization (release A)*. (Springer-Verlag, Berlin ; New York, 1992).
[11] J. Jensen and A. R. Mackintosh: *Rare earth magnetism: structures and excitations*. (Clarendon Press, Oxford, 1991).
[12] S. H. Liu, D. R. Behrendt, S. Legvold and R. H. Good: Phys. Rev. Vol. 116 (1959), p. 1464-1468.
[13] J. J. Rhyne: in *Magnetic Properties of Rare-Earth Metals*, edited by R. J. Elliot/Plenum Press, New York, (1972).
[14] S. B. Palmer and E. W. Lee: Proc. R. Soc. London, Ser. A Vol. 327 (1972), p. 519-&.
[15] H. Ott, C. Schussler-Langeheine, E. Schierle, G. Kaindl and E. Weschke: Appl. Phys. Lett. Vol. 88 (2006), p.
[16] J. Wenisch, C. Gould, L. Ebel, J. Storz, K. Pappert, M. J. Schmidt, C. Kumpf, G. Schmidt, K. Brunner and L. W. Molenkamp: Phys. Rev. Lett. Vol. 99 (2007), p. 077201.
[17] E. S. Lyons, R. C. O'Handley and C. A. Ross: J. Appl. Phys. Vol. 99 (2006), p. 08R105.
[18] K. Ha, M. Ciria, R. C. O'Handley, P. W. Stephens and S. Pagola: Phys. Rev. B Vol. 60 (1999), p. 13780-13785.
[19] M. T. Johnson, P. J. H. Bloemen, F. J. A. denBroeder and J. J. deVries: Rep. Prog. Phys. Vol. 59 (1996), p. 1409-1458.
[20] H. I. Smith: Physica E Vol. 11 (2001), p. 104-109.
[21] R. C. O'Handley: *Modern magnetic materials : principles and applications*. (Wiley, New York, 2000).
[22] B. B. Pant: J. Appl. Phys. Vol. 79 (1996), p. 6123-6125.
[23] S. Chikazumi: J. Appl. Phys. Vol. 32 (1961), p. S81-S82.
[24] J. F. Freedman: IBM J. Res. Dev. Vol. 6 (1962), p. 449-455.

Trends in Magnetism
10.4028/www.scientific.net/SSP.168-169

Magnetoelastic Effects in Nanostructures
10.4028/www.scientific.net/SSP.168-169.177

DOI References

[1] L. Krusin-Elbaum, T. Shibauchi, B. Argyle, L. Gignac and D. Weller: Nature Vol. 410 (2001), . 444-446.
doi:10.1038/35068515
[3] L. Berbil-Bautista, S. Krause, M. Bode, A. Badia-Majos, C. de la Fuente, R. Wiesendanger and . I. Arnaudas: Phys. Rev. B Vol. 80 (2009), p. 241408.
doi:10.1103/PhysRevB.80.241408
[6] J. C. Slonczewski: Phys. Rev. B Vol. 39 (1989), p. 6995-7002.
doi:10.1103/PhysRevB.39.6995
[7] D. Wortmann, S. Heinze, P. Kurz, G. Bihlmayer and S. Blugel: Phys. Rev. Lett. Vol. 86 (2001), . 4132-4135.
doi:10.1103/PhysRevLett.86.4132
[9] E. Callen and H. B. Callen: Phys. Rev. Vol. 139 (1965), p. A455-&.
doi:10.1103/PhysRev.139.A455
[12] S. H. Liu, D. R. Behrendt, S. Legvold and R. H. Good: Phys. Rev. Vol. 116 (1959), p. 1464- 468.
doi:10.1103/PhysRev.116.1464
[15] H. Ott, C. Schussler-Langeheine, E. Schierle, G. Kaindl and E. Weschke: Appl. Phys. Lett. Vol. 8 (2006), p.
doi:10.1063/1.2206699
[16] J. Wenisch, C. Gould, L. Ebel, J. Storz, K. Pappert, M. J. Schmidt, C. Kumpf, G. Schmidt, K. runner and L. W. Molenkamp: Phys. Rev. Lett. Vol. 99 (2007), p. 077201.
doi:10.1103/PhysRevLett.99.077201
[17] E. S. Lyons, R. C. O'Handley and C. A. Ross: J. Appl. Phys. Vol. 99 (2006), p. 08R105.
doi:10.1063/1.2176596
[18] K. Ha, M. Ciria, R. C. O'Handley, P. W. Stephens and S. Pagola: Phys. Rev. B Vol. 60 (1999), . 13780-13785.
doi:10.1103/PhysRevB.60.13780
[20] H. I. Smith: Physica E Vol. 11 (2001), p. 104-109.
doi:10.1016/S1386-9477(01)00184-9
[22] B. B. Pant: J. Appl. Phys. Vol. 79 (1996), p. 6123-6125.
doi:10.1002/cite.330680523
[1] L. Krusin-Elbaum, T. Shibauchi, B. Argyle, L. Gignac and D. Weller: Nature Vol. 410 (2001), p. 444-446.
doi:10.1038/35068515
[2] S. Krause, L. Berbil-Bautista, T. Hanke, F. Vonau, M. Bode and R. Wiesendanger: Europhys. Lett. Vol. 76 (2006), p. 637-643. L. Berbil-Bautista, S. Krause, M. Bode and R. Wiesendanger, Phys. Rev. B Vol. 76 (2007), p. 064411.
doi:10.1103/PhysRevB.76.064411
[3] L. Berbil-Bautista, S. Krause, M. Bode, A. Badia-Majos, C. de la Fuente, R. Wiesendanger and J. I. Arnaudas: Phys. Rev. B Vol. 80 (2009), p. 241408.

doi:10.1103/PhysRevB.80.241408
[4] M. Ciria, F. J. Castano, J. L. Diez-Ferrer, J. I. Arnaudas, B. G. Ng, R. C. O'Handley and C. A. Ross: Phys. Rev. B Vol. 80 (2009), p. 094417.
doi:10.1103/PhysRevB.80.094417
[16] J. Wenisch, C. Gould, L. Ebel, J. Storz, K. Pappert, M. J. Schmidt, C. Kumpf, G. Schmidt, K. Brunner and L. W. Molenkamp: Phys. Rev. Lett. Vol. 99 (2007), p. 077201.
doi:10.1103/PhysRevLett.99.077201